

Crossover from metal to insulator in dense lithium-rich compound CLi_4

 HPSTAR
 311-2016

 Xilian Jin^{a,1}, Xiao-Jia Chen^b, Tian Cui^{a,1}, Ho-kwang Mao^{b,c,1}, Huadi Zhang^a, Quan Zhuang^a, Kuo Bao^a, Dawei Zhou^d, Bingbing Liu^a, Qiang Zhou^a, and Zhi He^a
^aState Key Laboratory of Superhard Materials, College of Physics, Jilin University, Changchun 130012, China; ^bCenter for High Pressure Science and Technology Advanced Research, Shanghai 201203, China; ^cGeophysical Laboratory, Carnegie Institution of Washington, Washington, DC 20015; and ^dCollege of Physics and Electronic Engineering, Nanyang Normal University, NanYang 473061, China

Contributed by Ho-kwang Mao, December 29, 2015 (sent for review October 15, 2015; reviewed by Chang Q. Sun and Zhigang Wu)

At room environment, all materials can be classified as insulators or metals or in-between semiconductors, by judging whether they are capable of conducting the flow of electrons. One can expect an insulator to convert into a metal and to remain in this state upon further compression, i.e., pressure-induced metallization. Some exceptions were reported recently in elementary metals such as all of the alkali metals and heavy alkaline earth metals (Ca, Sr, and Ba). Here we show that a compound of CLi_4 becomes progressively less conductive and eventually insulating upon compression based on *ab initio* density-functional theory calculations. An unusual path with pressure is found for the phase transition from metal to semimetal, to semiconductor, and eventually to insulator. The Fermi surface filling parameter is used to describe such an antimetallization process.

high pressure | antimetallization | lithium-rich compound

Similar to the same first group element, hydrogen, lithium with a single valence electron is a good conductor of heat and metal at ambient conditions. It can transform from a nearly free-electron metallic solid to an insulating one, i.e., pressure-induced antimetallization (1–4). As a contrasting counterpart, lithium often provides a meaningful referential aspect for understanding hydrogen at high pressures (5). Hydrogen-rich materials of group-IV hydrides (6–10) are believed to be good candidates for the realization of metallization and even superconductivity at modest pressures much lower than that required for pure hydrogen due to “chemical precompression.” Whether group-IV lithium compounds hold similar expected outstanding properties to those of their same group hydrides becomes an interesting topic.

On the other hand, high-pressure studies delivered a completely unexpected antimetallization behavior for alkali metals such as Li (1, 3, 4) and Na (11). Charge transition from $2s$ to $2p$ of Li or Na itself was proposed to account for such a behavior. Being restricted to the pure elements in these cases, some underlying properties are covered. The multielement cases are needed to understand the feature of antimetallization from a different perspective at the fundamental level. For this purpose, the compounds of C_mLi_n are considered to be good examples for the understanding of the nature of physics (12–14). Examining their high-pressure behavior and exploring the possible metallization and superconductivity in this system are the focus of this work.

We have explored the crystal structures of lithium-rich compounds CLi_n in a wide pressure range from ambient pressure to 300 GPa. Fig. 1 shows the enthalpy-pressure curves of CLi_4 and the possible decomposition to the elements and compounds. The other possible lithium-rich carbides CLi_n ($n = 2 \sim 6$) and their stabilities can be found in *SI Appendix*, Fig. S1. Obviously, the compound of CLi_4 is stable at least above 3 GPa and below 300 GPa. Before about 3 GPa, CLi_4 is unstable and decomposes into a C_2Li_2 and Li mixture. After about 3 GPa, CLi_4 compounds become stable energetically over the decomposition enthalpy lines, and several different structures with a space group of $P1$ emerge with very close enthalpies. Fig. 2A exhibits the $P1$ cell with the lowest enthalpy. The other triclinic phase of $P-1$ phase becomes stable above 7 GPa,

which is obviously energetically favored over the others until the pressure close to 18 GPa. Subsequently, two monoclinic crystals of $P2_1$ and $C2/m$ appear in order, and the transformation occurs at 40 GPa. At 60 GPa, a high-symmetry phase of $R-3m$ appears and is stable until 128 GPa. Fig. 2E shows the structure with a hexagonal crystal lattice. There are three nonequivalent atoms, including two Li atoms and one C atom occupying the crystallographic $6c$ and $3b$ positions with $3m$ and $-3m$ site symmetry, respectively. Here, a pressure-induced symmetrization processes until 128 GPa is demonstrated from the low-symmetry phases to the high-symmetry one. After 128 GPa, another high-symmetry phase of $Fddd$ appears with 32 symmetry operators, which is slightly less than the 36 operators of $R-3m$. The orthorhombic phase consists of two nonequivalent atoms in the conventional cell, as shown in Fig. 2F. The Li atom occupies the crystallographic $32h$ position with the site symmetry of 1 , and the C atom locates at the $8a$ site with the site symmetry of 222 , respectively. Obviously, the six phases, i.e., $P1$, $P-1$, $P2_1$, $C2/m$, $R-3m$, and $Fddd$, are the most favored structures of CLi_4 compounds under pressure. The favored structures obtained in this work are shown in Fig. 2, and the corresponding parameters at respective pressures are listed in *SI Appendix*, Table S1.

The mechanical stability provides a useful understanding for the structure of crystals. The strain energy of a crystal must be positive against any homogeneous elastic deformations; i.e., the matrix of elastic constants C_{ij} must be positive definite (15). The elastic constants have been calculated and are listed in *SI Appendix*, Table S2. Obviously, the elastic constants of the structures satisfy the mechanical stability criteria (15, 16), indicating that the six structures are mechanically stable. The charts of phonon band structure and the phonon density of states for the proposed structures calculated at selected pressures are shown in *SI Appendix*, Fig. S2. The absence of the imaginary frequency modes indicates that these structures are stable dynamically. A direct result from the phonon density of states of these structures shows

Significance

The binary compound researched here enriches the studies of antimetallization just like in the pure elemental system, and the fundamental nature of matter in the subject has been expanded. During metallizing or antimetallizing in metallic states, the Fermi surface filling parameter is found to be a valuable parameter to quantify the evolution of the free electrons.

Author contributions: X.J. and T.C. designed research; X.J., X.-J.C., and T.C. performed research; X.J. contributed new reagents/analytic tools; X.J., X.-J.C., T.C., and H.-k.M. analyzed data; and X.J., X.-J.C., T.C., H.-k.M., H.Z., Q. Zhuang, K.B., D.Z., B.L., Q. Zhou, and Z.H. wrote the paper.

Reviewers: C.Q.S., Nanyang Technological University; and Z.W., Colorado School of Mines.

The authors declare no conflict of interest.

¹To whom correspondence may be addressed. Email: cuitian@jlu.edu.cn, jinxilian@jlu.edu.cn, or hmao@carnegiescience.edu.

This article contains supporting information online at www.pnas.org/lookup/suppl/doi:10.1073/pnas.1525412113/-DCSupplemental.

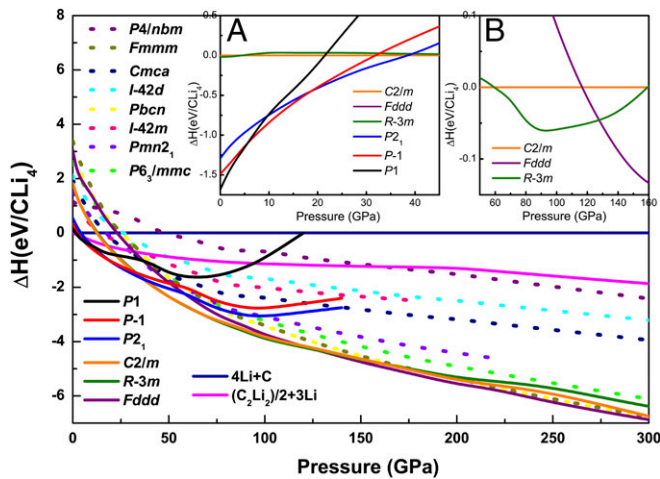


Fig. 1. Calculated enthalpy difference vs. pressure for various structures. Shown are enthalpies per CLi_4 unit of structures as functions of pressure with respect to the decomposition ($\text{C} + 4\text{Li}$ and $(\text{C}_2\text{Li}_2)/2 + 3\text{Li}$) enthalpies (royal blue and magenta lines, respectively), which are calculated by adopting the C, Li, and C_2Li_2 structures summarized in *SI Appendix, Table S1* at corresponding pressures. *Insets A and B* represent enthalpy difference curves with respect to the C2/m phase in the selected pressure ranges.

that the lighter Li atoms contribute more in frequency vibrational modes than the heavier C atoms.

It has been established that the standard ab initio density-functional theory (DFT) calculation usually gives an incorrect estimate of the fundamental energy band gap of materials (17). Contrary to the standard ab initio DFT calculations, ab initio DFT with the one-particle Green's function and the screened Coulomb interaction (*GW*) approximation shows good improvement in predicting the energy band gap. To obtain a reliable energy band structure of candidates, we have performed electronic band structure calculations at the level of the ab initio *GW* method. Comparing the up side of the 3D Fermi surface of $R-3m$ in Fig. 3 with the one in *SI Appendix, Fig. S3*, we can clearly find the difference between ab initio DFT calculation and the ab initio *GW* method. To investigate the degree of metallization quantitatively in metal CLi_4 under pressure, we define the Fermi surface filling parameter (FSFP) $\zeta = (1/N) \sum_{kn} \delta(\epsilon_{kn} - \epsilon_F) \propto N(0)/C\sqrt{\epsilon_F}$. Obviously, this parameter can be deduced from the nesting function $\xi(Q)$ (5). Here, $N(0)$ is the electron density of states at the Fermi level, and $C\sqrt{\epsilon_F}$ accounts for the intersection point between envelope and Fermi line in the chart of electron density of states of metal. This parameter can be used to describe the free electrons ratio in metal. Obviously, ζ is the maximum value of $\xi(Q)$ at the Γ point. This means that it can serve as a good measure of the degree of metallization.

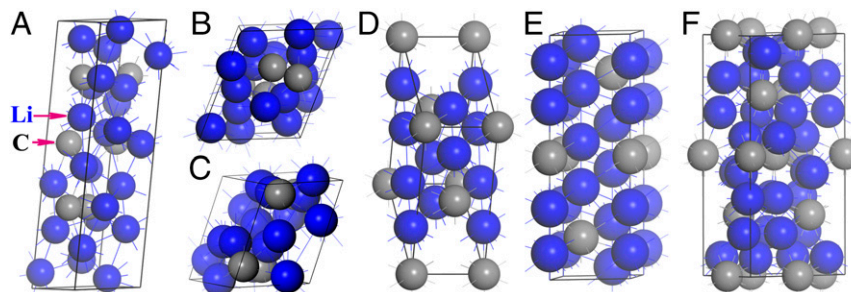


Fig. 2. The structures of CLi_4 under high pressures. (A) The $P1$ phase at 5 GPa; (B) the $P-1$ phase at 15 GPa; (C) the $P2$ phase at 30 GPa; (D) the C2/m phase at 40 GPa; (E) the $R-3m$ phase at 60 GPa; (F) the Fddd phase at 150 GPa. Black and blue atoms are C and Li, respectively.

A remarkable property of CLi_4 is the existence of phase transitions from metal to insulator with increasing pressure. At the lower pressure range below 70 GPa, $P1$, $P-1$, $P2$, C2/m , and $R-3m$ phases are all metallic, and the degree of metallization declines gradually with increasing pressure except a slight pressure-induced metallization from phase $P-1$ to $P2$, as described by FSFP ζ in Fig. 3, *Left*. At about 70 GPa, the metallic character of $R-3m$ CLi_4 disappears, and the nonmetallic character of the energy band gap appears. Above 70 GPa, the energy band gap of $R-3m$ phase gradually grows until reaching a value of 2.43 eV at 128 GPa with *GW* corrections, as shown in Fig. 3, *Right*. The $R-3m$ CLi_4 is a transitional phase from a metallic property to a non-metallic one. After 128 GPa, the insulated Fddd phase appears with a band gap of 3.26 eV at 128 GPa. With further increasing pressure, the band gap has a slight elevation until 300 GPa. The loss of metallization and increase of nonmetallic character in the compressed lithium-rich compound CLi_4 system can be reflected quantitatively by the FSFP ζ and electron energy band gaps.

Subsequently, calculations about electronic structures have been performed to reveal the emergence of antimetallization in the dense lithium-rich compound CLi_4 . Hybridizations of valence electrons have been discovered under pressure, shown in the partial density of states in Fig. 4 *A and B, Left*. At a lower pressure range, the interaction between valence electrons and ionic cores is weak, and the nonlocal electrons near Fermi energy account for the metallic property, as displayed in Fig. 4 *A, Center and Right*. From 3D and 2D electron localization function (ELF) shown in Fig. 4 *A*, we can see that the conductivity comes from connected regions where the value of ELF is about 0.5. But at higher pressures, volume contraction in the crystal lattice increasingly shortens interatomic distances, and hybrid electrons are repulsed by the core electrons into the lattice interstices, as shown in Fig. 4 *B, Center and Right*. Eventually, the nearly free electrons with the ELF value of 0.5 become totally localized and are confined to disconnected areas in interstitial positions of atoms as demonstrated by the 3D ELF and 2D ELF in Fig. 4 *B*.

The emergence of insulating CLi_4 can be understood in the framework of localized Wannier functions (WFs) and group theory described very recently (18). In the insulating Fddd phase, the valence band consisting of six branches splits off from the rest of the band structure in the vicinity of the band gap. The calculated wave functions corresponding to those from Γ_4^- to Γ_3^+ levels at Γ points can be found in the band structure in *SI Appendix, Fig. S4*. In the conventional cell, the centers of valence electronic charge coincide with three unoccupied Wyckoff positions, i.e., $16e$ (0.5795, 0.5000, 0.5000), $16f$ (0.5000, 0.6616, 0.5000), and $16g$ (0.5000, 0.5000, 0.4500), demonstrating that the valence band can be described by three sets of localized WF's centered exactly on those positions unoccupied by atoms. At high isosurfaces of 0.18, the bottom and top valence band wave functions Γ_4^- and Γ_3^+ represent a bonding combination of p -like orbitals centered on all of

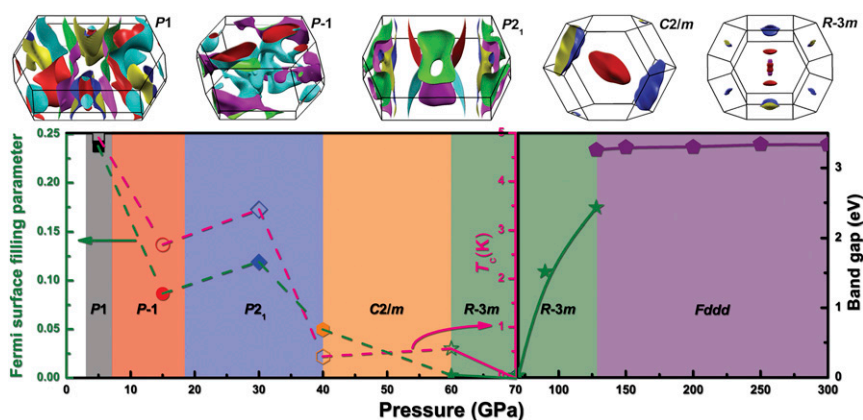


Fig. 3. Evolution of antimetallization properties and superconductivity with pressure. The evolution from metal to insulator is described quantitatively with FSFP (before 70 GPa; *Left*, olive green dashed line) and the electron energy band gap is shown (after 70 GPa; *Right*, olive green and purple solid lines), using ab initio GW calculations. The superconducting transition temperature T_c as a function of pressure is depicted with a pink dashed line (*Left*). The 3D Fermi surfaces are shown as the up side calculated by the GW method for the corresponding phases at selected pressures. The various background colors represent the pressure ranges of stable phases.

the C atoms. The p (Li- $2p$, C- $2p$) character of this band can also be found in other k regions of the Brillouin zone. The top valence band is mainly of p - p hybrids ($\sim 97\%$), and a small component of s (Li- $2s$, C- $2s$) character ($\sim 3\%$) can also be found in particular regions of reciprocal space. *SI Appendix, Fig. S4* demonstrates the contribution from Li- $2p$ along the high-symmetry points in the Brillouin zone. Our calculations show that the WF's center is not at midpoints of the lines joining neighboring Li atoms and reflects multicenter chemical bonding in the insulating state. Therefore, the insulating phase exhibits a multicenter p - p bonding property. These results reveal that the opening band gap is mainly due to strong p - p hybridization, which is controlled by symmetry principles. A similar situation takes place in the insulating phase of $R-3m$.

Lithium is well known for its ability to form heterogeneous clusters with various elements. Since the experimental discovery and theoretical verification of “hyperlithiated” bonding, which involves formal violations of the octet rule in doped Li clusters (19), there have been many theoretical and experimental investigations with the purpose of insight into the specific structural and electronic properties of these systems. Such systems include CLi_n (20, 21), etc. CLi_6 was first predicted (20) and later verified experimentally (21) to be stable with respect to dissociation into the stoichiometric CLi_4 and Li_2 molecules. To enhance the H_2 binding and attain high storage capacity, some nanostructures have been functionalized with polyolithiated molecules, e.g., CLi_4 for hydrogen storage. The stabilities of the designed functional materials for H_2 storage have been verified by means of molecular dynamics simulations (22).

Next we examine whether the predicted phases of this compound could be superconducting within the framework of BCS theory. The results are shown in Fig. 3, *Left*. The electron-phonon coupling parameter (EPC λ), the logarithmic average phonon frequency (ω_{log}), and the Eliashberg phonon spectral function [$\alpha^2F(\omega)$] are calculated at high pressures. The resulting EPC λ for $P1$, $P-1$, $P2_1$, $C2/m$, and $R-3m$ phases at 5 GPa, 15 GPa, 30 GPa, 40 GPa, 50 GPa, and 60 GPa are 0.533, 0.398, 0.425, 0.364, 0.276, and 0.212, respectively, indicating that the EPC is very weak. The superconducting transition temperature T_c can be estimated from the Allen–Dynes modified McMillan equation (23) $T_c = \frac{\omega_{\text{log}}}{1.2} \exp\left[\frac{1.04(1+\lambda)}{\lambda - \mu^*(1 - 0.62\lambda)}\right]$, which has been found to be highly accurate for many materials with $\lambda < 1.5$. The ω_{log} values can be calculated directly from the phonon spectra. The metallic phases mentioned above have ω_{log} of 305.75 K, 416.16 K, 400.64 K, 405.86 K, 484.95 K, and 560.85 K at selected pressures,

respectively. The Coulomb pseudopotential μ^* is often taken as 0.1 for most metals. Using μ^* of 0.1, the estimated T_c s are 4.725 K, 1.691 K, 2.344 K, 0.949 K, 0.094 K, and 0.001 K, respectively,

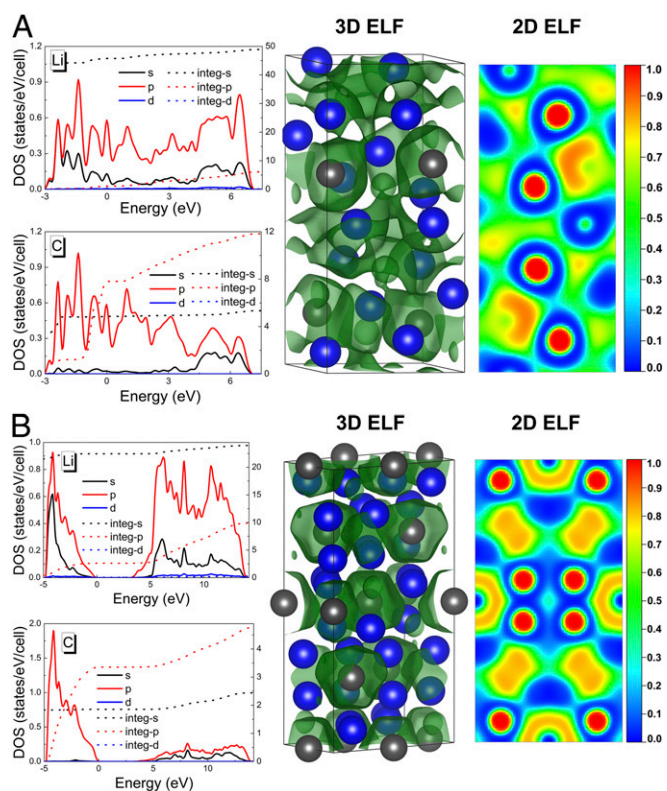


Fig. 4. Electronic structures of the CLi_4 phases at selected pressures. Blue and black atoms represent Li and C, respectively. (A) $P2_1$ phase at 30 GPa. A, *Upper Left* and *Lower Left* are the partial density of states (PDOS) and integrated PDOS of elements Li and C. A, *Center* shows a 3D electron localization function (3D ELF) map with the ELF value of 0.5, and A, *Right* is the corresponding 2D electron localization function (2D ELF) slice along the (001) plane. (B) $Fddd$ phase at 150 GPa. B, *Upper Left* and *Lower Left* shows PDOS and integrated PDOS of elements Li and C. B, *Center* represents 3D ELF with the ELF value of 0.5, and B, *Right* depicts corresponding 2D ELF for the (010) plane.

revealing a similar variation tendency with antimetallization with pressure.

The dense lithium-rich compound CLi_4 shows completely opposite behavior compared with the counterpart of group-IV hydrides under pressure, metallization in hydrides and antimetallization in CLi_4 , respectively. Pressure-induced antimetallization reported here is expected in not only pure elements but also multiple compounds, such as some alkali metal compounds. The binary compound researched here enriches the studies of antimetallization just like in the pure elemental system, and the fundamental nature of matter in the subject has been expanded. During metallizing or antimetallizing in metallic states, the Fermi surface filling parameter is found to be a valuable parameter to quantify the evolution of the free electrons.

Methods Summary

An ab initio evolutionary algorithm is used to search for the structure with the lowest energy at a given pressure with the implementation in USPEX code (24). The underlying ab initio structure relaxations were performed using DFT within the Perdew–Burke–Ernzerhof (PBE) parameterization of the generalized gradient approximation (GGA) (25) as implemented in the Vienna ab initio simulation package VASP code (26). The all-electron projector-augmented wave (PAW) method (27) is adopted with the PAW potentials taken from the VASP library, where $1s2s2p$ and $2s2p$ are treated as valence electron configurations for Li and C atoms, respectively. A plane-wave basis set with an energy cutoff of 1,000 eV is used. This gives good convergence of total energies.

The plane-wave pseudopotential method within the PBE-GGA, through the Quantum-ESPRESSO (QE) package (28), is used to study the lattice dynamics

and EPC. In the QE code, the favored phases from PAW calculations are fully reoptimized within a force and energy convergence threshold of 10^{-5} Ry/bohr and 10^{-6} Ry to minimize the internal force and energy, respectively. The Troullier–Martins norm-conserving pseudopotentials for Li and C are generated using the FHI98PP code (29) with $2s$ and $2s2p$ as valence electrons, respectively. The pseudopotentials are then carefully tested by comparing the calculated lattice parameter and electronic band structure with VASP codes. A convergence test gives the choice of kinetic energy cutoffs of 80 Ry, and the Monkhorst–Pack (MP) (30) grids of k -point sampling for each one favored phases using a grid of spacing $2\pi \times 0.025 \text{ \AA}^{-1}$ in the Brillouin zone (BZ). A density of q mesh with $2\pi \times 0.04 \text{ \AA}^{-1}$ in the first BZ is used in the interpolation of the force constants for the phonon dispersion curve calculations, and a denser mesh of $2\pi \times 0.025 \text{ \AA}^{-1}$ is used for the phonon density of states curve calculations. Subsequently, EPCs are calculated in the first BZ on the same MP q -point meshes, using individual EPC matrices obtained with a grid of spacing $2\pi \times 0.025 \text{ \AA}^{-1}$. All of the convergences of the plane-wave basis set and MP sampling are carefully examined by using higher kinetic energy cutoffs and denser grid sets.

ACKNOWLEDGMENTS. Parts of calculations were performed at the High Performance Computing Center (HPCC) of Jilin University. This work was supported by the National Basic Research Program of China (Grant 2011CB808200), the Program for Changjiang Scholars and Innovative Research Team in University (Grant IRT1132), the National Natural Science Foundation of China (Grants 51572108 and 11174102), the National Fund for Fostering Talents of Basic Science (Grant J1103202), the HeNan Joint Funds of the National Natural Science Foundation of China (Grant U1304612), and the Special Funding of National Natural Science Foundation of China for Theoretical Physics (Grant 11247222).

- Neaton JB, Ashcroft NW (1999) Pairing in dense lithium. *Nature* 400:141–144.
- Hanfland M, Syassen K, Christensen NE, Novikov DL (2000) New high-pressure phases of lithium. *Nature* 408(6809):174–178.
- Matsuoka T, Shimizu K (2009) Direct observation of a pressure-induced metal-to-semiconductor transition in lithium. *Nature* 458(7235):186–189.
- Yao Y, Tse JS, Klug DD (2009) Structures of insulating phases of dense lithium. *Phys Rev Lett* 102(11):115503.
- Kasinathan D, et al. (2006) Superconductivity and lattice instability in compressed lithium from Fermi surface hot spots. *Phys Rev Lett* 96(4):047004.
- Ashcroft NW (2004) Hydrogen dominant metallic alloys: High temperature superconductors? *Phys Rev Lett* 92(18):187002.
- Feng J, et al. (2006) Structures and potential superconductivity in at high pressure: En route to “metallic hydrogen”. *Phys Rev Lett* 96(1):017006.
- Chen XJ, et al. (2008) Superconducting behavior in compressed solid SiH_4 with a layered structure. *Phys Rev Lett* 101(7):077002.
- Chen XJ, et al. (2008) Pressure-induced metallization of silane. *Proc Natl Acad Sci USA* 105(1):20–23.
- Eremets MI, Trojan IA, Medvedev SA, Tse JS, Yao Y (2008) Superconductivity in hydrogen dominant materials: Silane. *Science* 319(5869):1506–1509.
- Ma Y, et al. (2009) Transparent dense sodium. *Nature* 458(7235):182–185.
- Ruschewitz U, Pottgen R (1999) Structural phase transition in Li_2C_2 . *Z Anorg Allg Chem* 625:1599–1603.
- Chen XQ, Fu CL, Franchini C (2010) Polymeric forms of carbon in dense lithium carbide. *J Phys Condens Matter* 22(29):292201.
- Nylén J, Konar S, Lazor P, Benson D, Häussermann U (2012) Structural behavior of the acetylide carbides Li_2C_2 and CaC_2 at high pressure. *J Chem Phys* 137(22):224507.
- Nye JF (1985) *Physical Properties of Crystals* (Oxford Univ Press, Oxford).
- Wu Z, et al. (2007) Crystal structures and elastic properties of superhard IrN_2 and IrN_3 from first principles. *Phys Rev B* 76(5):054115.
- Onida G, Reining L, Rubio A (2002) Electronic excitations: Density-functional versus many-body Green’s-function approaches. *Rev Mod Phys* 74:601–659.
- Naumov II, Hemley RJ (2015) Origin of transitions between metallic and insulating states in simple metals. *Phys Rev Lett* 114(15):156403.
- Schleyer PR, Würthwein EU, Pople JA (1982) Effectively hypervalent first-row molecules. 1. Octet rule violations by OLi_3 and OLi_4 . *J Am Chem Soc* 104:5839–5841.
- Schleyer PR, Würthwein EU, Kaufman E, Clark T, Pople JA (1983) Effectively hypervalent molecules. 2. Lithium carbide (CLi_3), lithium carbide (CLi_6), and the related effectively hypervalent first row-molecules, $\text{CLi}_5\text{-nH}_n$ and $\text{CLi}_{6-n}\text{H}_n$. *J Am Chem Soc* 105:5930–5932.
- Kudo H (1992) Observation of hypervalent CLi_6 by Knudsen-effusion mass spectrometry. *Nature* 355:432–434.
- Er S, Wijs GAd, Brocks G (2009) Hydrogen storage by polyolithiated molecules and nanostructures. *J Phys Chem C* 113:8997–9002.
- Allen PB, Dynes RC (1975) Transition temperature of strong-coupled superconductors reanalyzed. *Phys Rev B* 12:905–922.
- Oganov AR, Glass CW (2006) Crystal structure prediction using *ab initio* evolutionary techniques: Principles and applications. *J Chem Phys* 124(24):244704.
- Perdew JP, Burke K, Ernzerhof M (1996) Generalized gradient approximation made simple. *Phys Rev Lett* 77(18):3865–3868.
- Kresse G, Furthmüller J (1996) Efficient iterative schemes for *ab initio* total-energy calculations using a plane-wave basis set. *Phys Rev B Condens Matter* 54(16):11169–11186.
- Blöchl PE (1994) Projector augmented-wave method. *Phys Rev B Condens Matter* 50(24):17953–17979.
- Giannozzi P, et al. (2009) QUANTUM ESPRESSO: A modular and open-source software project for quantum simulations of materials. *J Phys Condens Matter* 21(39):395502.
- Fuchs M, Scheffler M (1999) *Ab initio* pseudopotentials for electronic structure calculations of poly-atomic systems using density-functional theory. *Comput Phys Commun* 119(1):67–98.
- Monkhorst HJ, Pack JD (1976) Special points for Brillouin-zone integrations. *Phys Rev B* 13:5188–5192.